

# Design of Hygroscopic Bioplastic Products Stable in Varying Humidities

Sirui Liu, Mercedes A. Bettelli, Xinfeng Wei, Antonio J. Capezza, Benedikt Sochor, Fritjof Nilsson, Richard T. Olsson, Eva Johansson, Stephan V. Roth, and Mikael S. Hedenqvist\*

Hygroscopic biopolymers like proteins and polysaccharides suffer from humidity-dependent mechanical properties. Because humidity can vary significantly over the year, or even within a day, these polymers will not generally have stable properties during their lifetimes. On wheat gluten, a model highly hygroscopic biopolymer material, it is observed that larger/thicker samples can be significantly more mechanically stable than thinner samples. It is shown here that this is due to slow water diffusion, which, in turn, is due to the rigid polymer structure caused by the double-bond character of the peptide bond, the many bulky peptide side groups, and the hydrogen bond network. More than a year is required to reach complete moisture saturation ( $\approx 10$  wt.%) in a 1 cm thick plate of glycerol-plasticized wheat gluten, whereas this process takes only one day for a 0.5 mm thick plate. The overall moisture uptake is also retarded by swelling-induced mechanical effects. Hence, hygroscopic biopolymers are better suited for larger/thicker products, where the moisture-induced changes in mechanical properties are smeared out over time, to the extent that the product remains sufficiently tough over climate changes, for example, throughout the course of a year.

biodegradable, has attractive mechanical properties, good film-forming properties, and excellent oxygen-barrier properties in dry conditions, and is available as a co-product from starch and ethanol-biofuel production.<sup>[1–13]</sup> Because of the latter, it is available at a comparatively low price and with a low variation in quality.<sup>[2,14]</sup> It is also not expected to yield the same microplastic problems as those found with today's plastics. Gluten readily polymerizes and crosslinks at elevated temperatures and when exposed to mechanical energy/impact (refer to dough-processing), which leads to a highly aggregated and cohesive material.<sup>[15–20]</sup> In the presence of a plasticizer, the cohesiveness leads to a tough plastic material.

However, proteins like WG and other hygroscopic biobased polymers, such as thermoplastic starch, suffer from moisture-sensitive mechanical properties – from stiffer, less tough behavior in a dry indoor winter climate to softer, more ductile/tough behavior in a moist summer period in, for


example, northern Europe. In Sweden, the indoor relative humidity in February can decline to 10% (absolute humidity outdoors:  $2 \text{ g cm}^{-3}$ ). The corresponding values in July can rise to more than 60% ( $\geq 10 \text{ g cm}^{-3}$ ) (Figure S1, Supporting

## 1. Introduction

Wheat gluten (WG) is a potential alternative to synthetic petroleum-based plastics for several reasons: It is biobased and

S. Liu, M. A. Bettelli, X. Wei, A. J. Capezza, F. Nilsson, R. T. Olsson, S. V. Roth, M. S. Hedenqvist  
Department of Fiber and Polymer Technology  
Polymeric Materials Division  
School of Engineering Sciences in Chemistry  
Biotechnology and Health  
KTH Royal Institute of Technology  
Stockholm 10044, Sweden  
E-mail: mikaelhe@kth.se

B. Sochor, S. V. Roth  
Deutsches Elektronen-Synchrotron  
DESY  
Notkestraße 85, D-22607 Hamburg, Germany  
E. Johansson  
Department of Plant Breeding  
Swedish University of Agricultural Sciences  
P.O. Box 190, Lomma SE-234 22, Sweden

 The ORCID identification number(s) for the author(s) of this article can be found under <https://doi.org/10.1002/mame.202200630>

© 2023 The Authors. Macromolecular Materials and Engineering published by Wiley-VCH GmbH. This is an open access article under the terms of the Creative Commons Attribution License, which permits use, distribution and reproduction in any medium, provided the original work is properly cited.

DOI: 10.1002/mame.202200630

Information). In fact, humidity can also change significantly over a day (Figure S1, Supporting Information), depending on the actual variations in temperature. This sometimes makes the mechanical properties sensitive over a shorter time scale. Because the changes in properties depend on water diffusion into and out of the material, the size of the variations is expected to depend on the geometry of the product, resulting in thinner paper-like applications being very sensitive, whereas thick and rigid materials will be less sensitive. The changes in properties over the year or within a day (or days) are thus expected to be less or more “smeared out” over time for larger/thicker products. This suggests that the materials can find better use in larger dimensioned applications over longer times, whereas thinner paper-like structures, if not encapsulated/protected, can more beneficially be used as, for example, sensors for thinner structures.

In this work, the aim was to determine if the observed more stable properties in thicker WG products could be directly related to the rate of the water/moisture transport (diffusivity). Glycerol-plasticized WG is a model material for highly hygroscopic biopolymers, in that it shows strong effects of moisture on, for example, mechanical properties.<sup>[16]</sup> Consequently, the influence of the product design (plates with a large range in thickness) on the water uptake kinetics was determined on glycerol-plasticized WG plates at zero and medium-high (50%) relative humidity (RH). The moisture-induced effects on the mechanical properties were discovered on plates using three-point bending and dynamic mechanical analysis. Also, of practical importance when one considers products of different sizes is the fact that the properties/structure of the biopolymer material is not significantly altered or that any product-size-dependent properties can be predicted/handled. Hence, the structural homogeneity of differently sized WG products was determined and assessed here using infrared spectroscopy and small-angle X-ray scattering (SAXS) and wide-angle (WAXS) X-ray spectroscopy.

## 2. Experimental Section

### 2.1. Materials and Manufacturing of the Samples

The WG powder was supplied by Lantmännen Reppe AB, Sweden. It consisted of  $86.3 \pm 0.3$  wt.% WG proteins ( $N \times 6.25$ ),  $5.8 \pm 0.1$  wt.% wheat starch,  $0.9 \pm 0.1$  wt.% fat, and  $0.8 \pm 0.1$  wt.% ash. Glycerol with a purity of 99.5% was supplied by P.W.G. Produkter AB, Sweden.

The plates were prepared by first mixing gluten, glycerol, and milli-Q water in a weight ratio of 70/30/4 in a kitchen mixer (WATT; DUKA AB, Sweden) until a homogeneous dough was obtained. The dough was dried before being flash-frozen in liquid  $N_2$  and ground (Retsch, Hann, Germany). The compression moulding of the plates was performed in a Fontijne Press (TP400, Barendrecht, Netherlands) between PTFE anti-sticking films.<sup>[21,22]</sup> Part of the calculated amount (to fill the specific mould) of ground WG was first premolded/compacted at room temperature and 250 kN press force for 1 min to exhaust air. After the pressure was released and the press plates of the hot press were separated, the residual calculated amount of WG was added and the temperature was raised to 130 °C. Another pre-molding step was then taken by moving the plates together (to reach 250 kN) and apart, three times, to exhaust residual air before the fi-



**Figure 1.** Pellets and cut plates with thicknesses of (from bottom to top) 0.5, 1.0, 3.0, 4.3, 6.1, and 10.6 mm.

nal pressing, which occurred at 130 °C at 250 kN for 15 min. Steel frames/moulds were used with thicknesses (and area dimensions) of 0.5 (diameter,  $\phi = 200$  mm), 1.0 ( $\phi = 200$ ), 3.0 ( $\phi = 200$ ), 4.3 ( $100 \times 100$ ), 6.1 ( $100 \times 100$ ), and 10.6 ( $100 \times 100$ ) mm to fabricate the plates. The exact thickness of each plate was measured using a Mitutoyo IDC-112B (Mitutoyo Scandinavia, Sweden) micrometer, and the average of three randomly positioned measurements was used. The samples were cut into  $20 \times 100$  mm<sup>2</sup> long strips by a cutting machine (Ryobi, China) (Figure 1). For the thickest sample (20 mm with either a square  $200 \times 200$  mm<sup>2</sup> cross-section or a cylinder cross-section with a diameter of 80 mm), the dough was pelletized using a plastic granulator (Meltic 280) and then pressed. The square 20 mm thick sample had a glycerol content of 28 wt.%.

### 2.2. Water Uptake

The plates were preconditioned at room temperature in an electric desiccator (Secador, USA) for at least 66 days before any measurement. This was referred to as the 0% RH condition in the remaining article. The loss in weight during storage at 0% RH (after the compression moulding) was obtained by intermittently removing the samples from the desiccator and measuring the weight on a Precisa XR 205-DR balance (Switzerland). The measurements were made on ten replicates. After the drying treatment, some samples were exposed to  $50 \pm 2.5\%$  RH at  $23 \pm 1^\circ\text{C}$  in a climate room and the weights were recorded as a function of time on a Mettler Toledo AE100 balance (Switzerland) to obtain water uptake curves. Three replicates were used in the water uptake experiment.

### 2.3. Dynamic Mechanical Analysis (DMA)

The dynamic mechanical properties of rectangular samples ( $20 \times 5$  mm<sup>2</sup>) were determined using a dynamic mechanical analyzer in tensile mode (TA instruments DMA, model Q800, USA). 0.5 mm thick plates, taken directly from the electric desiccator and also from conditioning at 50% RH for at least 48 h, were

used. The temperature was increased from  $-100$  to  $140$  °C at a heating rate of  $3$  °C  $\text{min}^{-1}$  using the tension clamp mode at a frequency of  $1$  Hz. The strain amplitude used was  $0.08\%$ . The damping ( $\tan\delta$ ) was calculated as the ratio of the loss modulus ( $E''$ ) and the storage modulus ( $E'$ ).

#### 2.4. Flexural Test

The mechanical properties of the samples were measured by 3-point bending (flexural test) using an Instron 5566 tensile tester (Instron Corp., USA) with a  $10$  kN load cell. The three-point bending test was carried out at  $50 \pm 2.5\%$  RH and  $23 \pm 1$  °C on samples conditioned at the same conditions for at least  $48$  h. Another set of samples was stored for  $66$  days in the electric desiccator before the measurements. The  $100$  mm long samples were bent with a flexural strain rate of  $0.1$  ( $\text{mm mm}^{-1}$ )  $\text{min}^{-1}$  using a support span of  $60$  mm. The flexural modulus, maximum stress, and strain at maximum stress were obtained according to ASTM D790 (2002).<sup>[23]</sup> According to the standard, the span-width-to-thickness ratio should be  $16$ . The sample closest to that was the  $4.3$  mm sample ( $\approx 14$ ); hence, it was evaluated here. However, for comparison reasons, the  $6.1$  mm sample was also evaluated. According to the standard, any mechanical values beyond  $5\%$  strain should not be used. However, the maximum stress and the strain at maximum stress were determined here but used only for comparison purposes to determine the effects of moisture.

#### 2.5. Infrared Spectroscopy (IR)

The infrared spectra were obtained with a Perkin-Elmer Spectrum 2000 FTIR spectrometer (Perkin Elmer Inc., USA) equipped with an MKII Golden Gate™ (Kent, England) attenuated total reflection (ATR) device. The scan resolution was set to  $4$   $\text{cm}^{-1}$ , with  $16$  scans obtained for each spectrum. In the spectral region from  $1700$  to  $1580$   $\text{cm}^{-1}$ , the samples' infrared absorbance spectra were deconvoluted using an enhancement factor  $\gamma$  of  $2$  and a smoothing filter of  $70\%$ , and then baseline-corrected.<sup>[9]</sup>

#### 2.6. SAXS and WAXS

All X-ray scattering experiments were performed at beamline P03,<sup>[24]</sup> which is part of the third-generation synchrotron source PETRA III (Deutsches Elektronen-Synchrotron DESY, Germany). The X-ray energy for all measurements was fixed at  $11.8$  keV. For the SAXS experiments, a Pilatus 2 M detector (Dectris, Switzerland) was used, while the WAXS data were recorded using a LAMBDA 9 M detector (X-Spectrum, Germany). The sample-detector distances were  $3152 \pm 1$  mm (SAXS) mm and  $212.0 \pm 0.1$  mm (WAXS). The distances were calibrated using Silver behenate (CAS-Nr.: 2489-05-6) and Lanthanum hexaboride (CAS-Nr.: 12008-21-8) standards (Merck, Darmstadt, Germany) for the SAXS and WAXS set-up, respectively. The data from both techniques were obtained separately and consecutively for all samples. Specimens were cut into rectangular thin slices representing the cross-section of the  $4.3$  and  $10.6$  mm thick samples and then mounted on Kapton duct tape (Goodfellow, Huntingdon, United Kingdom) to allow the X-ray beam to penetrate the

specimen perpendicular to the sliced specimen surface. For the  $0.5$  mm thick sample, the specimen was directly mounted to allow the X-ray beam to penetrate the specimen along its thickness. Several millimeters were mapped vertically and horizontally along the thin slice to verify its homogeneity and also to avoid radiation damage. The illumination time for each mapping point was  $1$  s. For data reduction and analysis, several scattering images were later summed up and background-subtracted using the diode counter values in the beamstop and the free software DPDAK<sup>[25]</sup> as well as standard scaling and correction routines.<sup>[26]</sup>

### 3. Results and Discussion

#### 3.1. Sample Size and the Effects of Moisture

It has been observed that thick samples of WG have significantly more stable mechanical properties than thinner samples. Not only does the use of  $20$  mm thick plates of glycerol-plasticized WG provide a product with high strength (shown in **Figure 2**, Video S1, Supporting Information), but also the apparent mechanical properties do not vary over the year.

However, the mechanical properties vary considerably for a small/thin sample with, for example, yearly variations in relative humidity. As observed in **Figure 3**, the stiffness ( $E'$ ) of the  $0.5$  mm sample was  $5$  times higher at  $0\%$  RH ( $\approx 375$  MPa) than it was at  $50\%$  RH ( $\approx 75$  MPa) at  $23$  °C. This change in stiffness is similar to what has been reported for WG-based materials under tensile testing.<sup>[16]</sup> The  $\tan\delta$  curve shows a low and high-temperature peak and an intermediate shoulder, as has also been observed in similar WG systems (with or without the intermediate shoulder) (**Figure 3**).<sup>[27,28]</sup> It has been suggested that this is due to the glass transition (peak relaxation) of three phases with, from low temperature to high temperature, decreasing glycerol content.<sup>[27]</sup> As in ref. [27], all three transitions were affected by the presence of water, which, due to plasticization, led to a shift of these to a lower temperature (**Figure 3**). It is suggested that the low-temperature transition is due to hydrogen bond interactions between the WG surface and partly phase-separated glycerol, involving also local motions of amino-side groups. The intermediate transition is considered to originate from cooperative and collective motions of strongly interacting (disulfide crosslinked) WG molecules. The high-temperature relaxation is suggested to be due to conformational/segmental movements of WG facilitated by a network of percolated plasticisers (mainly water).

#### 3.2. Water Uptake

The stable mechanical properties of the thick samples can be understood from the following water uptake analysis. The water diffusion uniaxially along the thickness ( $x$ ) of the sample can be expressed by Fick's second law:<sup>[29]</sup>

$$\frac{\partial C}{\partial t} = \frac{\partial}{\partial x} \left( D(C) \frac{\partial C}{\partial x} \right) \quad (1)$$

where  $t$  and  $C$  correspond to the diffusion time and the water concentration, respectively. At a high solute uptake (as in the case here with water in WG,  $9$ – $10$  wt.% (**Table 1**)), the diffusion coeffi-



**Figure 2.** A 20 mm thick square plate of glycerol-plasticized WG, exposed to a barbell with a 100 kg weight, and a 20 mm thick circular plate that has been run over by a car wheel exerting a load of  $\approx 500$  kg. The lower middle image shows that the shape of the square plate recovered to almost 100% after unloading.

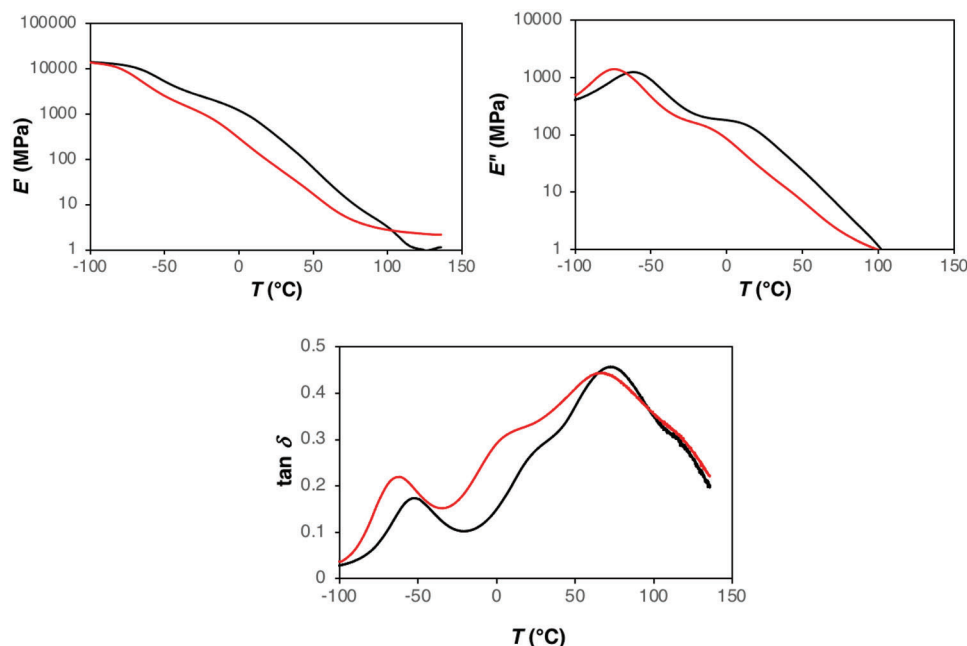


**Figure 3.** Dynamic mechanical data of the 0.5 mm thick plate conditioned at 0% RH (black curve) and 50% RH (red curve).

cient is solute concentration-dependent. The diffusivity can then be expressed as:<sup>[30]</sup>

$$D(C) = D_{C0} e^{\alpha_D C} \quad (2)$$

where  $D_{C0}$  is the zero-concentration diffusivity (the hypothetical water diffusivity in an unplasticized matrix) and  $\alpha_D$  is the water plasticization power. The latter is a measure of the plasticization efficiency of the solute (in this case, water).<sup>[31–33]</sup> The average diffusivity over the actual concentration range was calculated as:

$$D_A = \frac{D_{C0}}{C_f} \int_0^{C_f} e^{\alpha_D C} dC \quad (3)$$

where  $C_f$  is the final (saturation) surface concentration.

For a swelling system (i.e., when the solute uptake is large), the diffusion is more complex than it is in a system where the uptake is low.<sup>[34]</sup> In the initial part of the uptake in a plate geometry, the swelling occurs mainly in the thickness direction, as the unswollen core prohibits any expansion perpendicular to this direction (**Figure 4**). Once the solute reaches the core of the sample, the swelling becomes isotropic. This leads to an initial surface concentration ( $C_i$ ) that is lower than the final surface concentration, and the latter is approached by a rate  $\beta$ :

$$C(t) = C_i + (C_f - C_i) (1 - e^{-\beta t}) \quad (4)$$

The simulated concentration profiles, with the boundary condition given by Equation (4), were generated with the MATLAB software (Mathworks, USA) using a multi-step backward differ-



**Table 1.** Diffusion parameters.

Sample	$D_{C_0}$ [cm <sup>2</sup> s <sup>-1</sup> ]	$\alpha_D$ [1/wt.%] <sup>a)</sup>	$C_f$ [wt.%] <sup>b)</sup>	$C_i$ <sup>c)</sup>	$\beta$ [1/s]	$D_A$ [cm <sup>2</sup> s <sup>-1</sup> ]
0.5 mm	$1.97 \times 10^{-9}$	0.36	9.84	0.72	0.0003	$1.87 \times 10^{-8}$
3.0 mm	$1.97 \times 10^{-9}$	0.42	9.14	0.72	0.0004	$2.33 \times 10^{-8}$
Limonene/NR <sup>d)</sup>	$4.50 \times 10^{-7}$	0.005	360	0.44	0.00007	$1.26 \times 10^{-6}$
Water/NR <sup>e)</sup>	-	-	-	-	-	$3.0 \times 10^{-7}$
O <sub>2</sub> /NR <sup>f)</sup>	-	-	-	-	-	$1.5 \times 10^{-6}$

<sup>a)</sup> Unit: 100 g polymer g<sup>-1</sup> water; <sup>b)</sup> Unit: g water per 100 g polymer; <sup>c)</sup> Value relative to final value; <sup>d)</sup> Ref. [35]; <sup>e)</sup> Ref. [36]; <sup>f)</sup> Ref. [37].

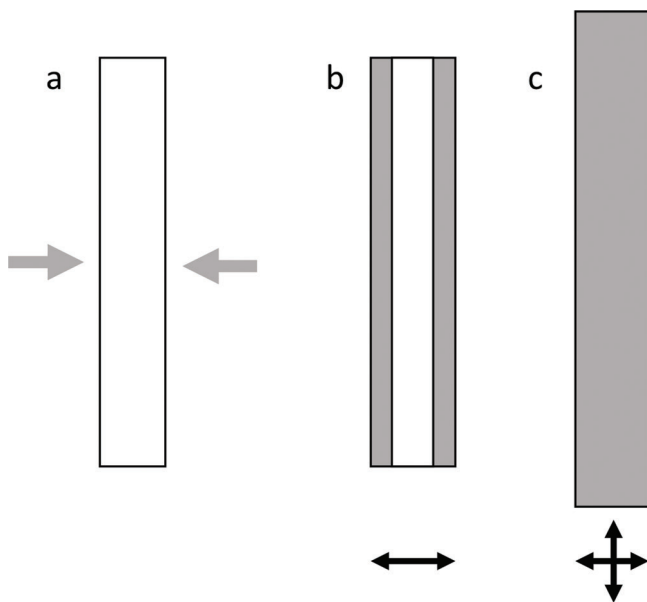


**Figure 4.** Illustration of the complex swelling behavior of a polymer plate exposed to a solute (side view). a) and b) 1D swelling, c) 3D swelling. Grey arrows indicate the solute sorption direction. Black arrows indicate the swelling directions. Grey parts indicate the solute-containing region of the sample.

entiation method<sup>[34]</sup> and integrated to yield the water uptake as a function of time. Because of symmetry, the condition at the center of the plate is a mirror boundary, meaning that the water concentration profile is always zero at that point. **Figure 5a** shows the best fit of the model to the experimental 0.5 mm plate uptake data, and the obtained diffusion parameters are given in Table 1. Observe the S-shaped uptake curve, which is due to the time-dependent surface concentration. **Figure 5c** shows the generated relatively steep water concentration profiles yielding the sorption curve in **Figure 5a**, which implies that when the thick samples were exposed to high RH for a short time, only a small region close to the sample surface was affected by water and the inner part was still dry.

Also, the experimental water uptake in a thicker sample (3 mm) was fitted with the numerical method (**Figure 5b**). The obtained set of parameter values was almost the same as those of the thinner sample (Table 1). It should be mentioned that, while the diffusion is clearly 1D in the 0.5 mm sample (the shortest distance perpendicular to the thickness direction was more than 10

times the thickness<sup>[29]</sup>), the situation is less evident in the 3 mm case. Nevertheless, based on the determined values (Table 1), the transport perpendicular to the thickness direction could be neglected in the latter thicker sample.

Using the obtained parameter values for the 0.5 and 3 mm samples, the time to reach the saturation/final moisture content, and half of this content, was calculated for the samples with different thicknesses (**Table 2**). The very slow saturation in the thicker samples was striking; the process takes quite a bit more than a year for an  $\approx 11$  mm thick plate. On the other hand, it takes only 1 day for a 0.5 mm thick plate. Hence, as the product/sample becomes larger, the effect of variations in humidity reduces. In fact, it may reduce to the extent that the product remains tough/ductile (if plasticized with, e.g., glycerol), despite the seasonal changes in humidity over the year. Notably, the 20 mm square plate shown in **Figure 2** would require  $\approx 4.5$  years to reach complete moisture saturation (at 50% RH and 23 °C), considering simply the saturation time of the 0.5 mm sample and the ratio of their thicknesses. However, using the 0.5 mm diffusion parameters in Table 1, the predicted moisture saturation of the 20 mm sample will be shorter. The latter is probably also more realistic due to that it includes the plasticization effects in more detail.

To put into perspective the slow diffusion of water in WG, the system was compared with a system of a molecularly flexible amorphous polymer that did not contribute any polar/dipolar or hydrogen bond interactions (non-polar lightly crosslinked natural rubber (NR)). The uptake/diffusion was here considered in three cases; i) the same polar solute as in the WG system (water), ii) a small non-swelling solute (oxygen), and iii) a swelling solute (limonene). In the case of water, the diffusivity in NR is around one order of magnitude higher than the average diffusivity in WG (Table 1) and the saturation and half-uptake times are 5 h (0.2 days) and 7 min (0.005 days), respectively, for a 0.5 mm thick plate (Table 2). The corresponding times for the 10.6 mm thick plate are 2 and 73 days. In the case of oxygen, the diffusivity in NR is around two orders of magnitude higher than the average water diffusivity in WG, and around one order of magnitude higher than the water diffusivity in NR (Table 1). Consequently, the times to saturation and half of the saturation uptake are 1 h and 1.5 min (0.001 days) (0.5 mm plate) and 10 h (0.4 days) and 20 days (10.6 mm plate) (Table 2). Finally, the swelling system (limonene in NR, **Figure 6d**) was considered, where now also the diffusion coefficient is concentration-dependent and a time-dependent surface concentration must be implemented. The zero-concentration diffusivity ( $D_{C_0}$ ) and average diffusivity

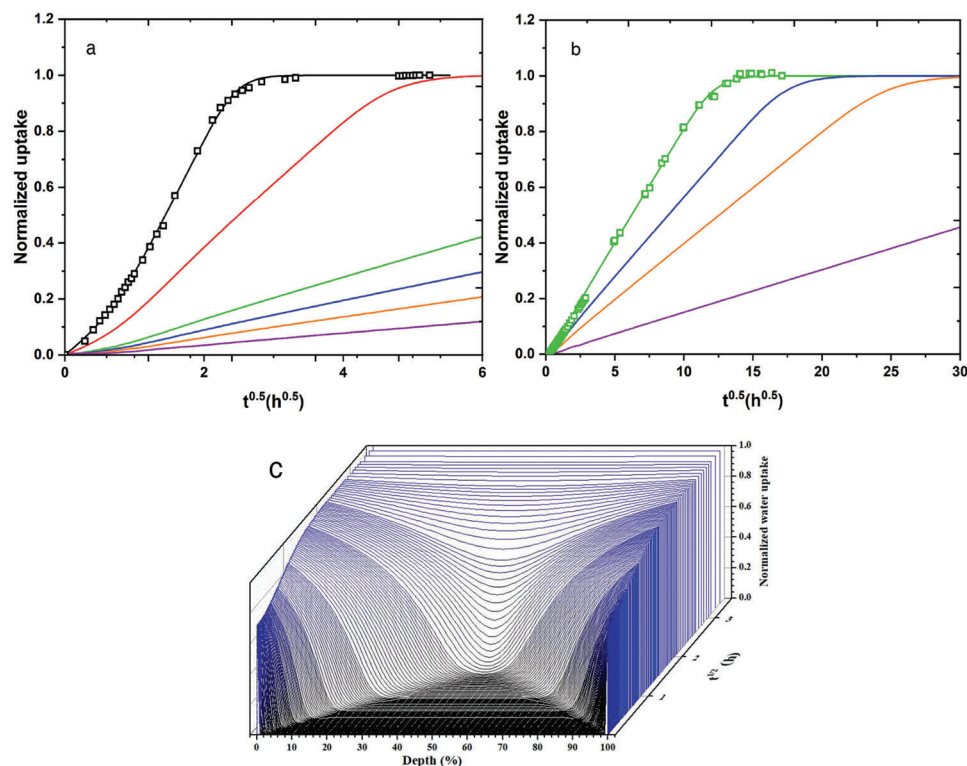


**Figure 5.** a) Experimental water uptake ( $\square$ ) and the fitted (black) curve for the 0.5 mm sample. The other curves represent the calculated uptake for the samples with (from left to right) thicknesses of 1.0, 3.0, 4.3, 6.1, and 10.6 mm. b) The same as in (a) but fitting the 3.0 mm sample uptake (green  $\square$ /curve). The other curves correspond to the calculated uptake for the 4.3, 6.1, and 10.1 samples. c) Generated water concentration profiles along the thickness corresponding to the fitted uptake in (a).

**Table 2.** Water uptake kinetics.

Thickness [mm]	0.5	1.0	3.0	4.3	6.1	10.6	
$t_{0.5}$ [days] <sup>a)</sup>	0.5 <sup>c)</sup>	0.1	0.3	2.1	4.2	8.7	44.7
	3.0 <sup>c)</sup>	-	-	1.6	3.2	6.7	25.6
$t_s$ [days] <sup>b)</sup>	0.5 <sup>c)</sup>	1.0	4.2	37.3	62.6	151.7	463.0
	3.0 <sup>c)</sup>	-	-	30.9	44.7	123.3	446.7
$t_{0.5}$ [days] <sup>a)</sup>	Limonene/NR	0.02	-	-	-	-	0.6
	Water/NR	0.005	-	-	-	-	2.1
	O <sub>2</sub> /NR	0.001	-	-	-	-	0.4
$t_s$ [days] <sup>b)</sup>	Limonene/NR	2	-	-	-	-	9
	Water/NR	0.2	-	-	-	-	73
	O <sub>2</sub> /NR	0.04	-	-	-	-	20

a) Time to reach half of the saturation uptake; b) Time to reach saturation uptake; c) Experimental data for the 0.5 or 3.0 mm thick plates were used to determine the uptake parameters. All data were calculated using the parameters in Table 1.

( $D_A$ ) are around two orders of magnitude higher for limonene in NR than for water in WG, despite the significantly larger size of limonene (Table 1). This shows the highly retarding effects of the system in which the matrix forms polar and hydrogen bonds with the solute and itself (water/WG) and the matrix chains are quite rigid (WG). The plasticization power of a solute is usually higher

when one starts from a rigid system (WG) as compared to a flexible system; this is reflected in the higher  $\alpha_D$  in the water/WG system than in the limonene/NR system (Table 1). The times to saturation and half saturation uptake of limonene in NR for the 10.6 mm plate are 9 days and 14 h (0.6 days), which are considerably shorter times than in the water/WG system. The corresponding times for the 0.5 mm plate are  $\approx$  2 h and 30 min (0.02 days). Notice here that the saturation uptake in the limonene/NR system takes twice as long as the saturation in the water/WG system. This is an effect of the time-dependent surface concentration, which has quite an impact, especially for the thinner plates, and retards the overall uptake/sorption. However, the long periods of time required to reach both the half-uptake and the saturation uptake of water in the thicker goods of the protein, which enables smearing out of the environment/climate-induced property changes, can be summarized as shown in Figure 6. The double-bond character of the peptide bond (due to the resonance effects of delocalized electrons) (a), the presence of bulky side groups on the peptide chains (b), and the presence of a hydrogen-bond network (with water molecules also present) (c) all contribute to the observed low moisture diffusivity.

### 3.3. Flexural Properties

For hygroscopic products exposed to a complex variation in relative humidity, depending on, for example, storage and shipping

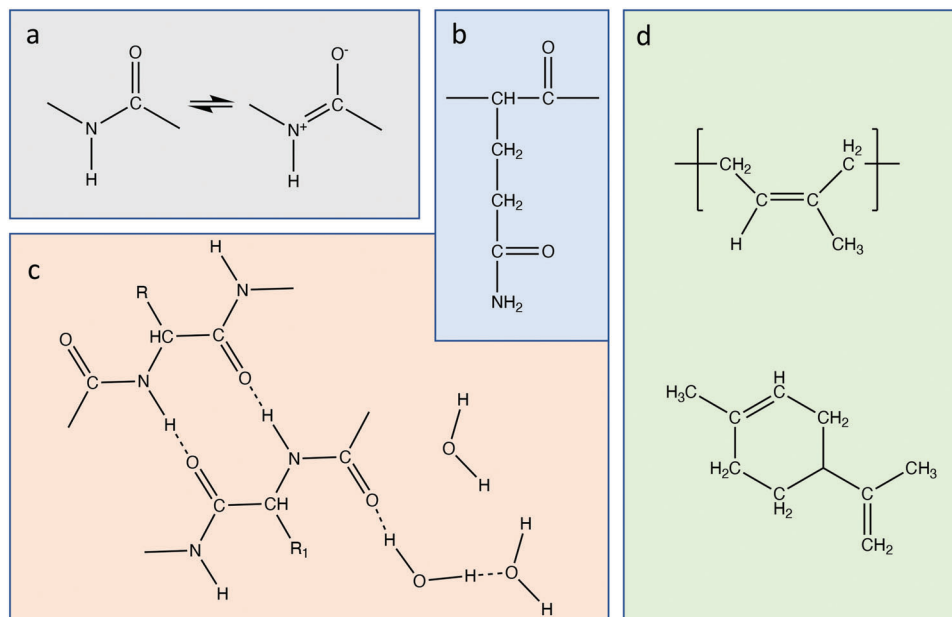


**Figure 6.** a) The resonance giving the peptide bond a double bond character, b) glutamine unit, c) illustration of hydrogen bonds (dashed lines), d) cis-1,4-polyisoprene (above) and limonene (below, without isomer details).

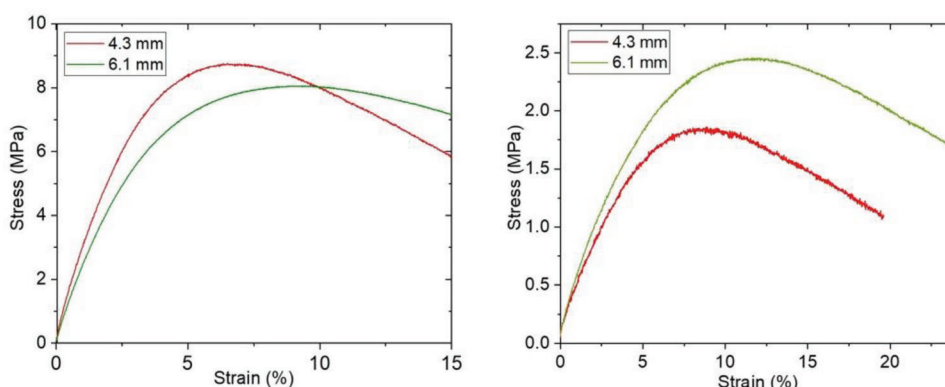


**Figure 7.** (left) Flexural stress-strain curves of plates stored at 0% RH after the pressing and (right) the corresponding flexural stress-strain curves of those conditioned at 50% RH.

conditions, it is difficult to predict the resulting mechanical properties due to the slow water diffusion in the material. This is illustrated here by measuring the flexural properties of the 4.3 and 6.1 mm thick samples, previously dried for 66 days (electric desiccator) after the compression molding, and also after additional conditioning at 50% RH for 48 h. **Figure 7a** shows typical flexural stress-strain curves for the 4.3 and 6.1 mm thick samples after the drying and **Figure 7b** shows the same curves for the same type of plates stored in the humid condition. The corresponding mechanical parameters are given in **Table 3**, with the estimated moisture content; the calculation of the latter is provided in the Supporting Information.

As expected, the stiffness and strength (maximum stress) were lower and the strain at maximum stress was higher in the moist condition. However, depending on the in- and outward slow water diffusion and the different geometries of the two samples, the relative size of the stiffness and strength for these were dif-

**Table 3.** Flexural properties of the 4.3 and 6.1 mm thick plates.

Sample	Moisture content [wt.%]	Flexure modulus [MPa]	Maximum stress [MPa]	Strain at max. stress [%]
0% RH				
4.3	0.5	291 ± 10	9.2 ± 0.2	6.6 ± 0.1
6.1	1.0	219 ± 7	8.0 ± 0.0	9.0 ± 0.1
50% RH				
4.3	4.2	38 ± 3	1.9 ± 0.1	8.9 ± 1.0
6.1	3.7	43 ± 5	2.1 ± 0.1	11.7 ± 0.0

ferent in the two conditions; the thinner sample was stiffer and stronger in the dry condition, whereas the stiffness and strength were higher for the thicker sample in the humid condition.

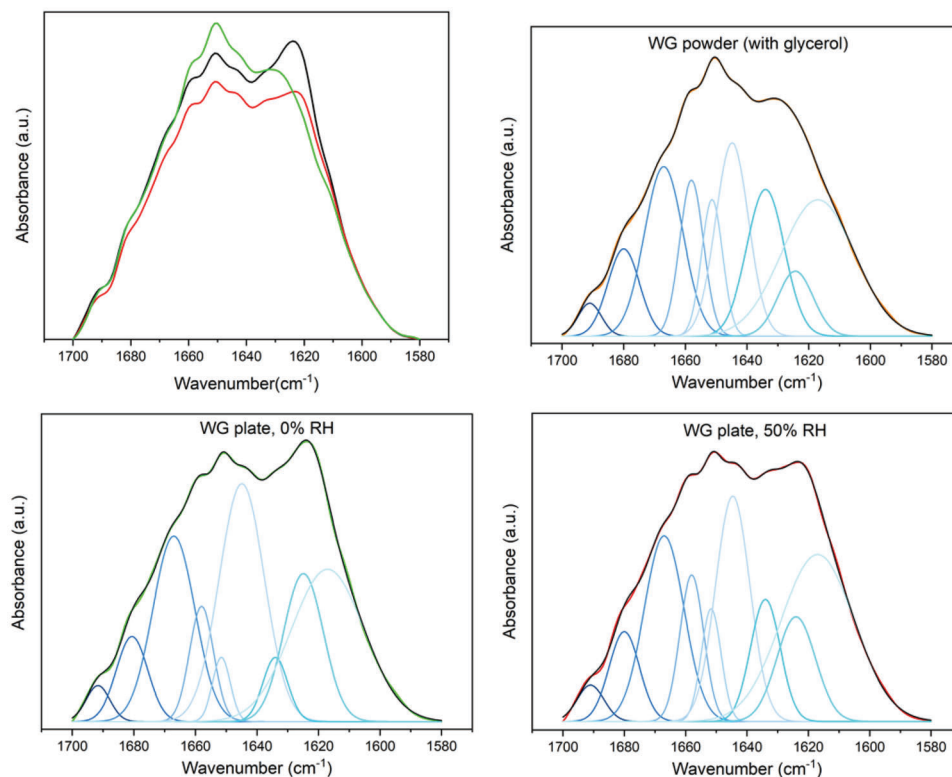


**Figure 8.** (upper left) Deconvoluted IR spectra in the amide I region of dry and moist 0.5 mm WG plate (black: 0% RH, red: 50% RH) and WG powder with glycerol (green). The remaining figures represent the deconvoluted experimental curves and the associated best fits using the 9 Gaussian bands.

**Table 4.** Relative contents of the secondary structures.

Secondary structure		The relative area of Gaussian peaks [%]		
Position /cm <sup>-1</sup>	Assignment	WG <sup>a)</sup> 0% RH	WG <sup>a)</sup> 50% RH	WG <sup>b)</sup> powder
1692, 1667	$\beta$ -Turns	19.5	18.8	17.9
1681, 1634	$\beta$ -Sheets, weakly hydrogen-bonded peptide groups	9.6	14.3	20.3
1658, 1651, 1644	$\beta$ -Helices and random coils	32.9	30.3	31.7
1625, 1618	$\beta$ -Sheets, strongly hydrogen-bonded peptide groups	38.0	36.5	30.1
	R <sup>2</sup> [%]	99.97	99.97	99.98

<sup>a)</sup> Pressed WG plates; <sup>b)</sup> Pristine powder mixed with glycerol.

### 3.4. Structure of the Protein Material

Above, the transport of water in different product/sample geometries (thicknesses) was considered and showed that when larger product dimensions were used, mechanical stability during variations in relative humidity increased. Now it is also important to understand whether larger dimensions affect the material structure, particularly the protein structure under compression molding.

First, the conformational structure of the protein was investigated. The IR absorption in the Amide I region is sensitive to changes in the protein secondary structure. The amide C=O stretching generates the amide I band, with minor contributions from the N-H vibration.<sup>[38]</sup> The deconvoluted Amide I band was

fitted/resolved into 9 peaks, as illustrated in **Figure 8**, and the relative contents of the different secondary structures are given in **Table 4**.<sup>[9,39–41]</sup> High-temperature treatment usually leads to denaturation and subsequent aggregation of the protein. Protein aggregation leads to an increase of tightly packed molecules, preferably in strongly hydrogen-bonded  $\beta$ -sheets. As observed in Table 4, the content of this structure also increased after the hot pressing. The presence of water (50% RH) yielded a slightly lower content of the strongly bonded  $\beta$ -sheets, possibly because water interferes with the protein hydrogen bonds.<sup>[42]</sup> However, care should be taken when evaluating the 50% RH data because water also absorbs in the Amide I region. To assess the conformational homogeneity within and between samples of different sizes, a large number of IR spectra were recorded on the 0.5, 4.3,



and 10.6 mm thick samples (typical spectra are given in Figure 8). In Figure S2 (Supporting Information), measurements at three random points on each of the two surfaces of the 0.5 mm sample showed very little difference, if any. Infrared spectra similar to those observed for the 0.5 mm sample were seen, with little variation, at the two facets of the 4.7 mm sample (Figure S3a, Supporting Information). However, the spectra taken in the interior of the sample were slightly different, with lower intensity in the region where strongly hydrogen-bonded  $\beta$ -sheets were observed ( $\approx 1620$ -region) (Figure S3b, Supporting Information). The thickest sample (10.6 mm) showed spectra more similar to those of the interior of the 4.3 mm sample in both the surface and the interior regions (Figure S4, Supporting Information). However, overall, the differences were relatively small and all samples and sampling positions represented an aggregated protein due to the high-temperature pressing. This is observed as a high absorption toward lower wavenumbers in the amide I region (strongly hydrogen-bonded  $\beta$ -sheet region) compared to the higher wavenumber region ( $\alpha$ -helix/unordered region,  $\approx 1650$   $\text{cm}^{-1}$ ) (Figure 8, upper left image).

The SAXS and WAXS analysis and modeling are described in the Supporting Information. The effects of humidity and plasticizers on the nanostructure and mechanical properties of wheat gluten materials using SAXS and WAXS have been fundamentally investigated previously.<sup>[3,16]</sup> The SAXS curves of the different samples (0.5, 4.3, or 10.6 mm) or the sampling points always showed the same features. Typical curves are given in Figure 9b, showing a broad peak/shoulder, in accordance with previous work.<sup>[43–45]</sup> In the curves in Figure 9b and Figure S5a,c,e (Supporting Information), the peak ( $d_1$ ) corresponded to a domain size of  $7.8 \pm 0.1$  nm (0.5 mm sample thickness),  $7.6 \pm 0.1$  nm (4.3 mm), and  $7.9 \pm 0.1$  nm (10.6 mm), respectively. The differences in domain size between the samples were small and did not show an observable trend. The full-width-half-maximum (FWHM) is a measure of the domain size distribution. Within the FWHM of all these peaks, the peak position and widths can be regarded as identical. The domain has been referred to as a poorly developed aggregated protein/glycerol structure,<sup>[44]</sup> which is also reflected in the high FWHM values (see Table S1, Supporting Information). A hexagonally ordered superstructure that has been observed with SAXS in several different WG systems (such as WG with urea or in gliadin systems)<sup>[46]</sup> was not observed here, which is expected for pure WG/glycerol systems.

The WAXS curves showed two broad peaks, corresponding to, respectively, a repeat distance of  $d_2 \approx 0.88 \pm 0.01$  nm and  $d_3 \approx 0.43 \pm 0.01$  nm ( $d_j = 2\pi/q_j$ ) (Figure 9c).  $q_j$  denote the maxima in the WAXS curves. The first distance has been ascribed to an inter- $\alpha$ -helix distance,<sup>[44]</sup> but can also represent an inter- $\beta$ -sheet distance. The second distance has been ascribed to an average backbone repeating distance within  $\alpha$ -helices but is also due to the average closest inter-atomic distance. Surprisingly, the 10.6 mm sample had a sharp/narrow peak at  $d_1 \approx 1.59 \pm 0.01$  nm. Because both the other peaks stay present, this seems to indicate a new and pronounced correlation length inside the system. To our knowledge, this has not been observed for WG systems before. Further work is needed to determine its precise origin and why it appeared for only the largest/thickest sample. However, its shape suggests a highly repeating “crystalline”-like molecular order. Finally, it should be noted that both the SAXS and WAXS curves

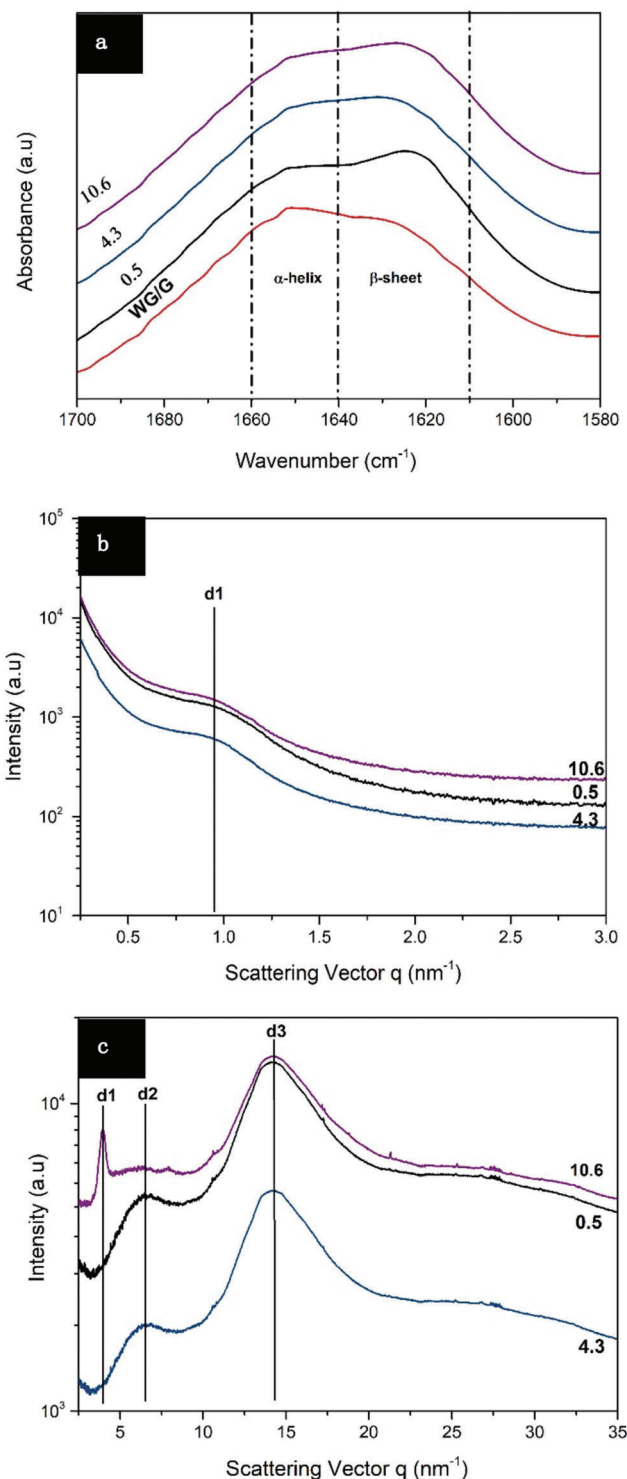


**Figure 9.** Typical IR (a), SAXS (b), and WAXS (c) curves of three samples with different thicknesses (in mm). WG/G refers to the pristine WG powder mixed with 30 wt.% glycerol (ambient conditions).

showed the same features among all replicates (not shown), indicating that the pressed materials were structurally homogeneous.

#### 4. Conclusion

It is shown here, on the model protein material, that when products are made/designed with larger geometries/sizes, the slow water diffusion (significantly slower than in a non-polar polymer matrix) leads to moisture-dependent mechanical properties that vary less (are smeared out) with variations in relative humidity (e.g., over a year). This, in turn, leads to products with constant/climate-independent mechanical properties, facilitating the use of hygroscopic polymers in many more applications than is the case today. One example is in types of furniture in, for example, cupboard shelves. As shown from DMA on the thinnest sample, the consequences of a complete uptake of water from a fully dried material (the thinnest sample) led to a decrease in stiffness by a factor of 5. This effect can, hence, be minimized by producing larger/thicker products. Often, materials are exposed to a complicated history of variations in relative humidity, and the flexural data here demonstrated that it is challenging to determine beforehand the resulting mechanical properties in such environments.

However, larger product dimensions may affect the structure of the material, due to, for example, thermal gradients during the processing of the material, especially if it is a complex protein material that aggregates/polymerizes at higher temperatures. It is shown here, though, based on a large number of measurements with IR, SAXS, and WAXS on WG samples with a large range in thickness, that the structure was not significantly altered, therefore not affecting the thickness dependence.

To conclude, when one creates products with larger geometries, the effects of seasonal or even daily variations in humidity on the material's performance can be reduced significantly or even eliminated in a material in which water transport is quite slow, such as (highly polar) protein plastics.

#### Supporting Information

Supporting Information is available from the Wiley Online Library or from the author.

#### Acknowledgements

Oscar Enrique Flores Peña was thanked for providing the WG dough mixtures. Formas (2019-00557, Sweden, Mercedes Bettelli), Erasmus+ Scholarship and Grand Est Scholarship (EU, France, Sirui Liu), and Bo Rydins Stiftelse (F30/19, Sweden, Antonio Capezza) are acknowledged for providing financial support. After initial online publication, the spelling of the second affiliation "Deutsches Elektronen-Synchrotron DESY" was corrected on February 14, 2023.

#### Conflict of Interest

The authors declare no conflict of interest.

#### Data Availability Statement

The data that support the findings of this study are available from the corresponding author upon reasonable request.

#### Keywords

biopolymers, diffusion, moisture, relative humidity, wheat gluten

Received: October 30, 2022  
Revised: December 12, 2022  
Published online: January 15, 2023

- [1] K. Joyce, G. T. Georgina, Y. Bozkurt, A. Pandit, *Signal Transduction Targeted Ther.* **2021**, *6*, 175.
- [2] W. S. Veraverbeke, J. A. Delcour, *Crit. Rev. Food Sci. Nutr.* **2002**, *42*, 179.
- [3] W. Qiong, R. L. Andersson, T. Holgate, E. Johnsson, U. W. Gedde, R. T. Olsson, M. S. Hedenqvist, *J. Mater. Chem. A* **2014**, *2*, 20996.
- [4] A. J. Capezza, Y. Cui, K. Numata, M. Lundman, W. R. Newson, R. T. Olsson, E. Johansson, M. S. Hedenqvist, *Adv. Sustain. Syst.* **2020**, *4*, 2000110.
- [5] M. S. Mathew, J. Davis, K. Joseph, *Analyst* **2018**, *143*, 3841.
- [6] A. J. Capezza, E. Robert, M. Lundman, W. R. Newson, E. Johansson, M. S. Hedenqvist, R. T. Olsson, *Polymers* **2020**, *12*, 459.
- [7] A. J. Capezza, M. Lundman, R. T. Olsson, W. R. Newson, M. S. Hedenqvist, E. Johansson, *Biomacromolecules* **2020**, *21*, 1709.
- [8] P. Baishya, D. Nath, P. Begum, R. C. Deka, T. K. Maji, *Eur. Polym. J.* **2018**, *100*, 137.
- [9] S.-W. Cho, M. Gällstedt, E. Johansson, M. S. Hedenqvist, *Int. J. Biol. Macromol.* **2011**, *48*, 146.
- [10] S. Tuntachon, A. Sukolrat, A. Numnuam, K. Kaewtatip, *Powder Technol.* **2019**, *351*, 66.
- [11] J. M. Lagarón, A. López-Rubio, M. José Fabra, *J. Appl. Polym. Sci.* **2016**, *133*, 42971.
- [12] I. Burešová, L. Hřivna, *Appl. Energy* **2011**, *88*, 1205.
- [13] W.-Y. Liu, J.-T. Zhang, T. Miyakawa, G.-M. Li, R.-Z. Gu, M. Tanokura, *Sci. Rep.* **2021**, *11*, 5206.
- [14] J.-P. Lens, L. A. De Graaf, W. M. Stevels, C. H. J. T. Dietz, K. C. S. Verhelst, J. M. Vereijken, P. Kolster, *Ind. Crops Prod.* **2003**, *17*, 119.
- [15] R. Kuktaite, H. Larsson, E. Johansson, *J. Cereal Sci.* **2004**, *40*, 31.
- [16] S. Yu, F. Chen, Q. Wu, S. V. Roth, K. Brüning, K. Schneider, R. Kuktaite, M. S. Hedenqvist, R. S. V., *ACS Sustainable Chem. Eng.* **2016**, *4*, 3388.
- [17] K. Bruyninckx, K. J. A. Jansens, B. Goderis, J. A. Delcour, M. Smet, *Eur. Polym. J.* **2015**, *68*, 573.
- [18] K. Bruyninckx, K. J. A. Jansens, J. A. Delcour, M. Smet, *Ind. Crops Prod.* **2016**, *81*, 38.
- [19] H. Türe, M. Gällstedt, R. Kuktaite, E. Johansson, M. S. Hedenqvist, *Soft Matter* **2011**, *7*, 9416.
- [20] T. Ogawa, Y. Matsumura, *Nat. Commun.* **2021**, *12*, 1708.
- [21] S. Sun, Y. Song, Q. Zheng, *Food Hydrocolloids* **2008**, *22*, 1006.
- [22] K. Kaewtatip, V. Tanrattanakul, T. Kaewtatip, *Key Eng. Mater.* **2013**, *531–532*, 321.
- [23] *Standard Test Methods for Flexural Properties of Unreinforced and Reinforced Plastics and Electrical Insulating Materials*, ASTM International, West Conshohocken, PA **2002**.
- [24] G. Santoro, A. Buffet, R. Döhrmann, S. Yu, V. Körstgens, P. Müller-Buschbaum, U. Gedde, M. Hedenqvist, S. V. Roth, *Rev. Sci. Instrum.* **2014**, *85*, 043901.
- [25] G. Benecke, W. Wagermaier, C. Li, M. Schwartzkopf, G. Flucke, R. Hoerth, I. Zizak, M. Burghammer, E. Metwalli, P. Müller-Buschbaum, M. Trebbin, S. Förster, O. Paris, S. V. Roth, P. Fratzl, *J. Appl. Crystallogr.* **2014**, *47*, 1797.
- [26] B. R. Pauw, A. J. Smith, T. Snow, N. J. Terrill, A. F. Thünemann, *J. Appl. Crystallogr.* **2017**, *50*, 1800.
- [27] A. Duval, S. Molina-Boisseau, C. Chirat, M.-H. Morel, *J. Appl. Polym. Sci.* **2016**, *133*, 43254.

- [28] S. Sun, Y. Song, Q. Zheng, *Food Hydrocolloids* **2007**, *21*, 1005.
- [29] U. W. Gedde, M. S. Hedenqvist, M. Hakkarainen, F. Nilsson, O. Das, *Applied Polymer Science*, Springer-Nature, Berlin, **2021**.
- [30] M. S. Hedenqvist, M. Krook, U. W. Gedde, *Polymer* **2002**, *43*, 3061.
- [31] J. -C. Huang, H. Liu, Y. I. Liu, *Int. J. Polym. Mater.* **2001**, *49*, 15.
- [32] E. Lin, X. You, R. M. Kriegel, R. D. Moffitt, R. C. Batra, *Polymer* **2017**, *115*, 273.
- [33] X-F. Wei, E. Linde, M. S. Hedenqvist, *npj Mater. Degrad.* **2019**, *3*, 18.
- [34] M. S. Hedenqvist, U. W. Gedde, *Polymer* **1999**, *40*, 2381.
- [35] J. E. Ritums, M. S. Hedenqvist, G. Bergman, T. Prodan, I. Emri, *Polym. Eng. Sci.* **2005**, *45*, 1194.
- [36] M. Hedenqvist, A. Angelstok, L. Edsberg, P. T. Larsson, U. W. Gedde, *Polym. J.* **1996**, *37*, 2887.
- [37] P. Danwanichakul, S. Jaroenkarn, P. Jumpathi, D. Dechojarassri, *Songklanakarin J. Sci. Technol.* **2006**, *28*, 5.
- [38] F. Dousseau, M. Pézolet, *Biochemistry* **1990**, *29*, 8771.
- [39] D. M. R. Georget, P. S. Belton, *Biomacromolecules* **2006**, *7*, 469.
- [40] N. Wellner, E. N. C. Mills, G. Brownsey, R. H. Wilson, N. Brown, J. Freeman, N. G. Halford, P. R. Shewry, P. S. Belton, *Biomacromolecules* **2005**, *6*, 255.
- [41] K. Kłosok, R. Welc, E. Fornal, A. Nawrocka, *Molecules* **2021**, *26*, 508.
- [42] N. Wellner, P. S. Belton, A. S. Tatham, *Biochem. Eng. J.* **1996**, *319*, 741.
- [43] F. Rasheed, M. S. Hedenqvist, R. Kuktaite, T. S. Plivelic, M. Gällstedt, E. Johansson, *Ind. Crops Prod.* **2015**, *73*, 90.
- [44] R. Kuktaite, T. S. Plivelic, H. Türe, M. S. Hedenqvist, M. Gällstedt, S. Marttila, E. Johansson, *RSC Adv.* **2012**, *2*, 11908.
- [45] F. Rasheed, W. R. Newson, T. S. Plivelic, R. Kuktaite, M. S. Hedenqvist, M. Gällstedt, E. Johansson, *RSC Adv.* **2014**, *4*, 2051.
- [46] F. Rasheed, W. R. Newson, T. S. Plivelic, R. Kuktaite, M. S. Hedenqvist, M. Gällstedt, E. Johansson, *Int. J. Biol. Macromol.* **2015**, *79*, 151.